Acta Cryst E CRYSTALLOGRAPHIC COMMUNICATIONS

ISSN 2056-9890

Crystal structure of bis{5-(4-chlorophenyl)-3-[6-(1*H*-pyrazol-1-yl)pyridin-2-yl]-1*H*-1,2,4-triazol-1-ido}nickel(II) methanol disolvate

Kateryna Znovjyak,[a] Sergiu Shova,[b] Dmitriy M. Panov,[c] Nataliia S. Kariaka,[a] Igor O. Fritsky,[a] Sergey O. Malinkin[a] and Maksym Seredyuk[a]*

[a]Department of Chemistry, Taras Shevchenko National University of Kyiv, Volodymyrska Street 64, Kyiv, 01601, Ukraine, [b]Department of Inorganic Polymers, "Petru Poni" Institute of Macromolecular Chemistry, Romanian Academy of Science, Aleea Grigore Ghica Voda 41-A, Iasi 700487, Romania, and [c]ChemBioCenter, Kyiv National Taras Shevchenko University, Kyiv 02094, 61 Winston Churchill Street, Ukraine. *Correspondence e-mail: mlseredyuk@gmail.com

Received 1 October 2024
Accepted 23 October 2024

Edited by B. Therrien, University of Neuchâtel, Switzerland

Keywords: crystal structure; nickel(II) complexes; neutral complexes; tridentate ligands; bisazolepyridines.

CCDC reference: 2393088

Supporting information: this article has supporting information at journals.iucr.org/e

The unit cell of the title compound, $[Ni(C_{16}H_{10}ClN_6)_2]\cdot 2CH_3OH$, consists of a neutral complex and two methanol molecules. In the complex, the two tridentate 2-(3-(4-chlorophenyl)-1*H*-1,2,4-triazol-5-yl)-6-(1*H*-pyrazol-1-yl)pyridine ligands coordinate to the central Ni^{II} ion through the N atoms of the pyrazole, pyridine and triazole groups, forming a pseudooctahedral coordination sphere. Neighbouring tapered molecules are linked through weak C—H(pz)···π(ph) interactions into monoperiodic chains, which are further linked through weak C—H···N/C interactions into diperiodic layers. The intermolecular contacts were quantified using Hirshfeld surface analysis and two-dimensional fingerprint plots, revealing the relative contributions of the contacts to the crystal packing to be H···H 32.8%, C···H/H···C 27.5%, N···H/H···N 15.1%, and Cl···H/H···Cl 14.0%. The average Ni—N bond distance is 2.095 Å. Energy framework analysis at the HF/3–21 G theory level was performed to quantify the interaction energies in the crystal structure.

1. Chemical context

A broad class of coordination compounds is represented by 3*d*-metal complexes based on tridentate bisazolepyridine ligands (Halcrow *et al.*, 2019; Suryadevara *et al.*, 2022), which find application in many fields, for example in catalysis (Xing *et al.*, 2014; Wei *et al.*, 2015) and molecular magnetism (Suryadevara *et al.*, 2022). In the case of asymmetric ligand design, where one of the azole groups carries a hydrogen on a nitrogen heteroatom and acts as a Brønsted acid, deprotonation can compensate for the charge of the central ion and in some cases form neutral complexes (Seredyuk *et al.*, 2014; Grunwald *et al.*, 2023). The periphery of the complexes also plays an important role, determining the way the molecules interact with each other, influencing the intermolecular connectivity, interaction energy and the organization of the crystal.

Encouraged by our interest in spin-transition complexes of 3*d*-metals formed by N-heterocyclic ligands (Seredyuk *et al.*, 2006, 2007; Bonhommeau *et al.*, 2012; Piñeiro-López *et al.*, 2018), we report a new neutral Ni^{II} complex based on an asymmetric deprotonated ligand with a monosubstituted phenyl group, 2-{5-[5-(4-chlorophenyl)-1*H*-1,2,4-triazol-3-yl]-6-(1*H*-pyrazol-1-yl)pyridine}, which continues our enduring project on the study of metal complexes of bisazolepyridines.

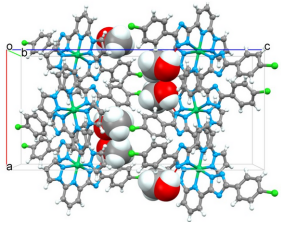

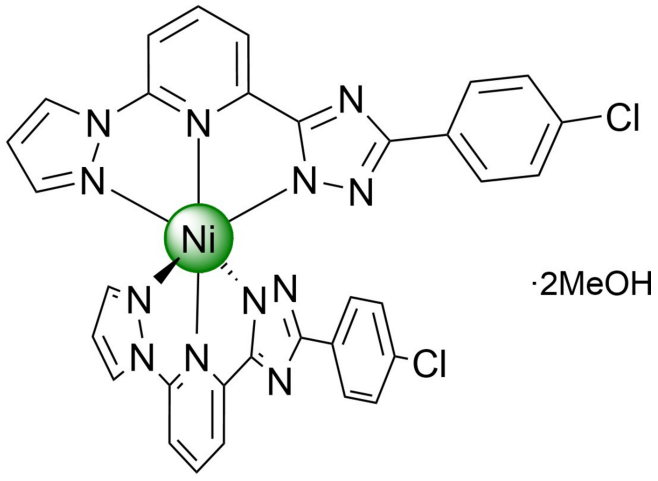

2. Structural commentary

The complex has a tapered structure with divergent phenyl groups. The phenyl group of the ligand is rotated by 26.2 (1)° relative to the pyrazole-pyridine-triazole (pz-py-trz) fragment, the arrangement of which is almost planar. There are two methanol molecules per complex, forming O—H···N hydrogen bonds with the trz rings (Fig. 1, Table 1). The central Ni ion has a distorted octahedral N_6 coordination environment formed by the nitrogen donor atoms of two tridentate ligands. The average Ni—N bond length is 2.095 Å. The average trigonal distortion parameters $\Sigma = \Sigma_1^{12}(|90 - \varphi_i|)$, where φ_i is the angle N—Ni—N′ (Drew *et al.*, 1995), and $\Theta = \Sigma_1^{24}(|60 - \theta_i|)$, where θ_i is the angle generated by superposition of two opposite faces of an octahedron (Chang *et al.*, 1990) are 119.4 and 387.3°, respectively. The values reveal a deviation of the coordination environment from an ideal octahedron (where $\Sigma = \Theta = 0$), which is, however, in the expected range for bisazolepyridine and similar ligands (see below). The calculated continuous shape measures [CShM(O_h)] value relative to the ideal octahedral symmetry is 3.714 (Kershaw Cook *et al.*, 2015). The volume of the [NiN_6] coordination polyhedron is 11.583 Å^3.

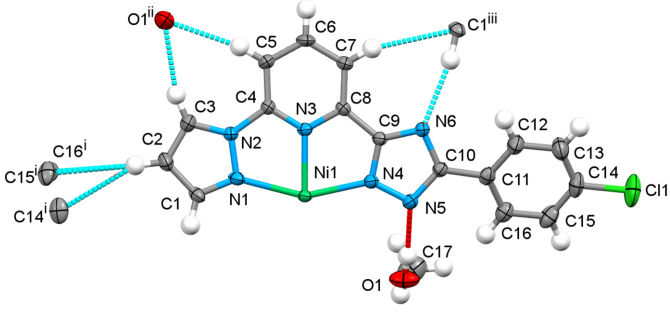

Figure 1
The molecular structure of half of the title compound, with displacement ellipsoids drawn at the 50% probability level. The strong O—H···N (red) and weak C–H···N/C/O (cyan) hydrogen bonds are shown with the nearest neighbours. Symmetry codes: (i) $1 - x, 1 + y, \frac{3}{2} - z$; (ii) $-\frac{1}{2} + x, \frac{1}{2} + y, \frac{3}{2} - z$; (iii) $\frac{1}{2} + x, \frac{1}{2} + y, \frac{3}{2} - z$.

Table 1
Hydrogen-bond geometry (Å, °).

D—H···A	D—H	H···A	D···A	D—H···A
C2—H2···C14^{i}	0.95	2.86	3.73 (4)	153
C2—H2···C15^{i}	0.95	2.74	3.686 (4)	178
C2—H2···C16^{i}	0.95	2.88	3.743 (4)	151
C3—H3···O1^{ii}	0.95	2.35	3.259 (4)	160
C5—H5···O1^{ii}	0.95	2.47	3.399 (4)	167
C1—H1···N6^{iii}	0.95	2.31	3.245 (6)	170
C7—H7···C1^{iii}	0.95	2.70	3.611 (4)	161
O1—H1*A*···N5	0.84	1.96	2.795 (6)	176

Symmetry codes: (i) $-x + 1, y + 1, -z + \frac{3}{2}$; (ii) $x + \frac{1}{2}, y + \frac{1}{2}, -z + \frac{3}{2}$; (iii) $x - \frac{1}{2}, y + \frac{1}{2}, -z + \frac{3}{2}$.

3. Supramolecular features

As a result of the tapered structure, neighbouring complexes are embedded in each other and interact through weak C–H(pz)···π(ph) intermolecular contacts between the pyrazole and phenyl groups [the C2···C_g(ph) distance is 3.534 Å]. They form one-dimensional supramolecular chains extending along the *b*-axis direction with a stacking periodicity equal to 10.1523 (4) Å (= cell parameter *b*) (Fig. 2). Weak intermolecular C—H(pz, py)···N/C(pz, trz) interactions, ranging from 3.245 (4) to 3.743 (4) Å (Table 1), connect neighbouring chains into two-dimensional layers along the *ab* plane. The voids between the layers are occupied by solvent molecules, which also participate in the bonding within separate layers. The methanol molecules form a strong O—H···N hydrogen bond with the deprotonated trz groups and weak hydrogen bonds C—H···O with the pz and py groups of the ligand. A complete list of selected intermolecular interactions is provided in Table 1.

4. Hirshfeld surface and two-dimensional fingerprint plots

Hirshfeld surface analysis was performed and the associated two-dimensional fingerprint plots were generated using

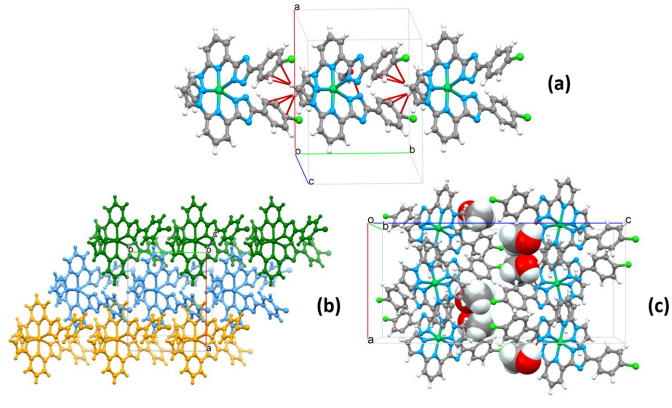

Figure 2
(*a*) A fragment of the monoperiodic supramolecular column formed by stacking of molecules along the *b* axis; (*b*) supramolecular diperiodic layers formed by stacking of the supramolecular columns in the *ac* plane. For a better representation, each column has a different colour; (*c*) stacking of the diperiodic layers along the *b* axis with the methanol molecules (CPK model) in the voids.

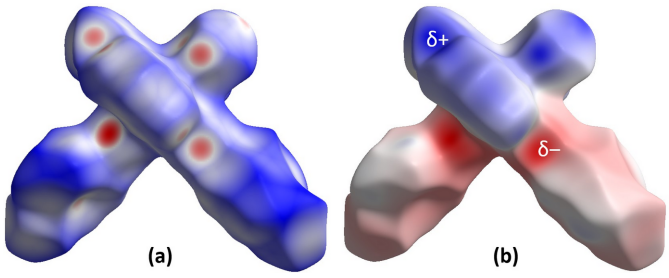

Figure 3
(*a*) A projection of d_{norm} mapped over the Hirshfeld surfaces, showing the intermolecular interactions within the molecule. Red/blue and white areas represent regions where contacts are shorter/larger than the sum and close to the sum of the van der Waals radii, respectively; (*b*) electrostatic potential for the title compound mapped over the Hirshfeld surface. Red/blue and white areas represent regions where the charge is negative/positive or close to zero.

CrystalExplorer (Spackman *et al.*, 2021), with a standard resolution of the three-dimensional d_{norm} surfaces plotted over a fixed colour scale from −0.6356 (red) to 1.6114 (blue) a.u. The pale-red spots symbolize short contacts and negative d_{norm} values on the surface corresponding to the interactions described above. The overall two-dimensional fingerprint plot is illustrated in Fig. 3*a*. The two-dimensional fingerprint plots, with their relative contributions to the Hirshfeld surface mapped over d_{norm}, are shown for the H···H, C···H/H···C, N···H/H···N and Cl···H/H···Cl contacts in Fig. 4. At 32.8%, the largest contribution to the overall crystal packing is from H···H interactions, which are located in the middle region of the fingerprint plot. C···H/H···C contacts contribute 27.5%, and Cl···H/H···Cl 14.0%, resulting in pairs of characteristic wings. The N···H/H···N contacts, represented by a pair of sharp spikes in the fingerprint plot, make a 15.1% contribution to the surface. The electrostatic potential energy calculated using the HF/3-21G basis is mapped on the Hirshfeld surface (Fig. 3*b*). The negative charge localizes on the trz-ph moiety and the Cl atom of the complex, while the pz-py moiety is relatively positively charged, which justifies the stacking of the molecules in columns and packing of the columns in diperiodic two-dimensional layers.

5. Energy frameworks analysis

The energy framework (Spackman *et al.*, 2021), calculated using the wave function at the HF/3-21G theory level, including the electrostatic potential forces (E_{ele}), the dispersion forces (E_{dis}) and the total energy diagrams (E_{tot}), is shown in Fig. 5. The cylindrical radii, adjusted to the same scale factor of 100, are proportional to the relative strength of the corresponding energies. The major contribution is due to the dispersion forces (E_{dis}), reflecting dominating interactions in the crystal of the neutral molecules. The topology of the energy framework resembles the topology of the interactions within and between layers described above. The calculated value E_{tot} for the intrachain interactions is −47.0 kJ mol^{-1} and for interchain interactions is down to −93.9 kJ mol^{-1}. The interlayer interactions have an energy of −31.9 kJ mol^{-1}. The colour-coded interaction mappings within a radius of 3.8 Å from the complex, together with full information on the various contributions to the total energy (E_{ele}, E_{pol}, E_{dis}, E_{rep}) are shown in the table in Fig. 5.

6. Database survey

A search of the Cambridge Structural Database (CSD, Version 5.42; Groom *et al.*, 2016) reveals several similar neutral 3*d* M^{II} complexes with tridentate bisazolepyridine ligands with a deprotonated azole group, for example, of Ni^{II}: YOCFAZ (Yuan *et al.*, 2014), ZOCKOT (Xing *et al.*, 2014), and ZOTVIP (Wei *et al.*, 2015); of Fe^{II}: EGIDIL (Seredyuk *et al.*, 2024), LUTGEO (Senthil Kumar *et al.*, 2015), and XODCEB (Shiga *et al.*, 2019). In addition, two related complexes based on phenanthroline-benzimidazole, DOMQUT (Seredyuk *et al.*, 2014) and dipyridylpyrrol,

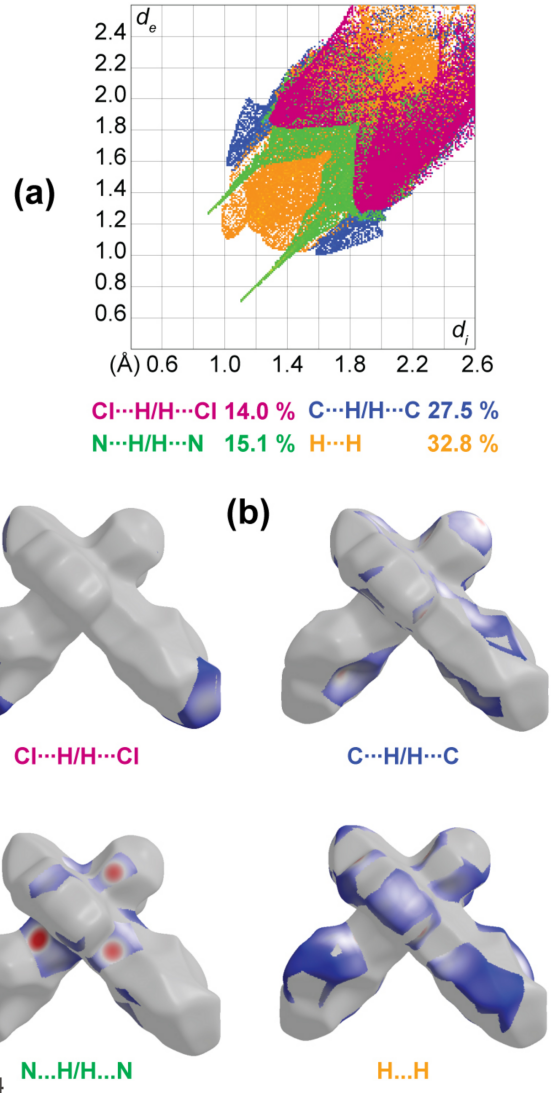

Figure 4
(*a*) Decomposition of the two-dimensional fingerprint plot into specific interactions; (*b*) a projection of d_{norm} mapped on the Hirshfeld surfaces, showing the intermolecular interactions within the molecule. Red/blue and white areas represent regions where contacts are shorter/larger than the sum and close to the sum of the van der Waals radii, respectively.

Table 2
Computed distortion indices (Å, °) for the title compound and for similar complexes reported in the literature.

CSD Refcode	Metal ion	<*M*—*N*>[a]	Σ	Θ	CShM(O_h)
Title compound	Ni	2.095	119.4	387.3	3.71
YOCFAZ	Ni	2.088[b]	120.8[b]	397.6[b]	3.65[b]
ZOCKOT	Ni	2.086	121.0	375.9	3.78
ZOTVIP	Ni	2.110	124.9	382.4	3.55
EGIDIL	Fe	1.955	89.8	314.6	2.25
EGIDIL02	Fe	2.167	146.8	492.8	5.28
LUTGEO	Fe	1.933	85.0	309.6	2.10
XODCEB	Fe	1.950	87.4	276.6	1.93
DOMQUT	Fe	1.991	88.5	320.0	2.48
DOMQUT02	Fe	2.183	139.6	486.9	5.31
NIRLOT	Fe	1.939	77.3	255.6	1.68

Notes: (*a*) averaged value; (*b*) value is averaged for two independent molecules.

NIRLOT (Grunwald *et al.*, 2023) were found. The values of the trigonal distortion indices and the CShM(O_h) values vary according to the length of the *M*—N distances, with shorter distances being systematically smaller. Table 2 collates the structural parameters of the complexes and of the title compound.

7. Synthesis and crystallization

The synthesis of the title compound was identical to that reported for a similar complex (Seredyuk *et al.*, 2022). It was produced by using a layering technique in a standard test tube. The layering sequence was as follows: the bottom layer contained a solution of $[Ni(L_2)](ClO_4)_2$ prepared by dissolving *L* = 2-[3-(4-chlorophenyl)-1*H*-1,2,4-triazol-5-yl]-6-(1*H*-pyrazol-1-yl)pyridine (89 mg, 0.274 mmol) and $Ni(ClO_4)_2\cdot 6H_2O$ (50 mg, 0.137 mmol) in boiling acetone, to which chloroform (5 ml) was then added. The middle layer was a methanol–chloroform mixture (1:10) (10 ml), which was covered by a layer of methanol (10 ml), to which 100 ml of NEt_3 were added dropwise. The tube was sealed, and violet plate-like single crystals appeared after 2 weeks (yield *ca* 65%). Elemental analysis calculated for $C_{34}H_{28}Cl_2N_{12}NiO_2$: C, 53.29; H, 3.68; N, 21.94. Found: C, 53.64; H, 3.42; N, 21.67.

8. Refinement

Crystal data, data collection and structure refinement details are summarized in Table 3. H atoms were refined as riding [C—H = 0.95–0.98 Å with U_{iso}(H) = 1.2–1.5U_{eq}(C)], while the O-bound H atom was refined freely with U_{iso}(H) = 1.5U_{eq}(O).

Acknowledgements

Author contributions are as follows: Conceptualization, KZ and MS; methodology, KZ; formal analysis, DMP; synthesis,

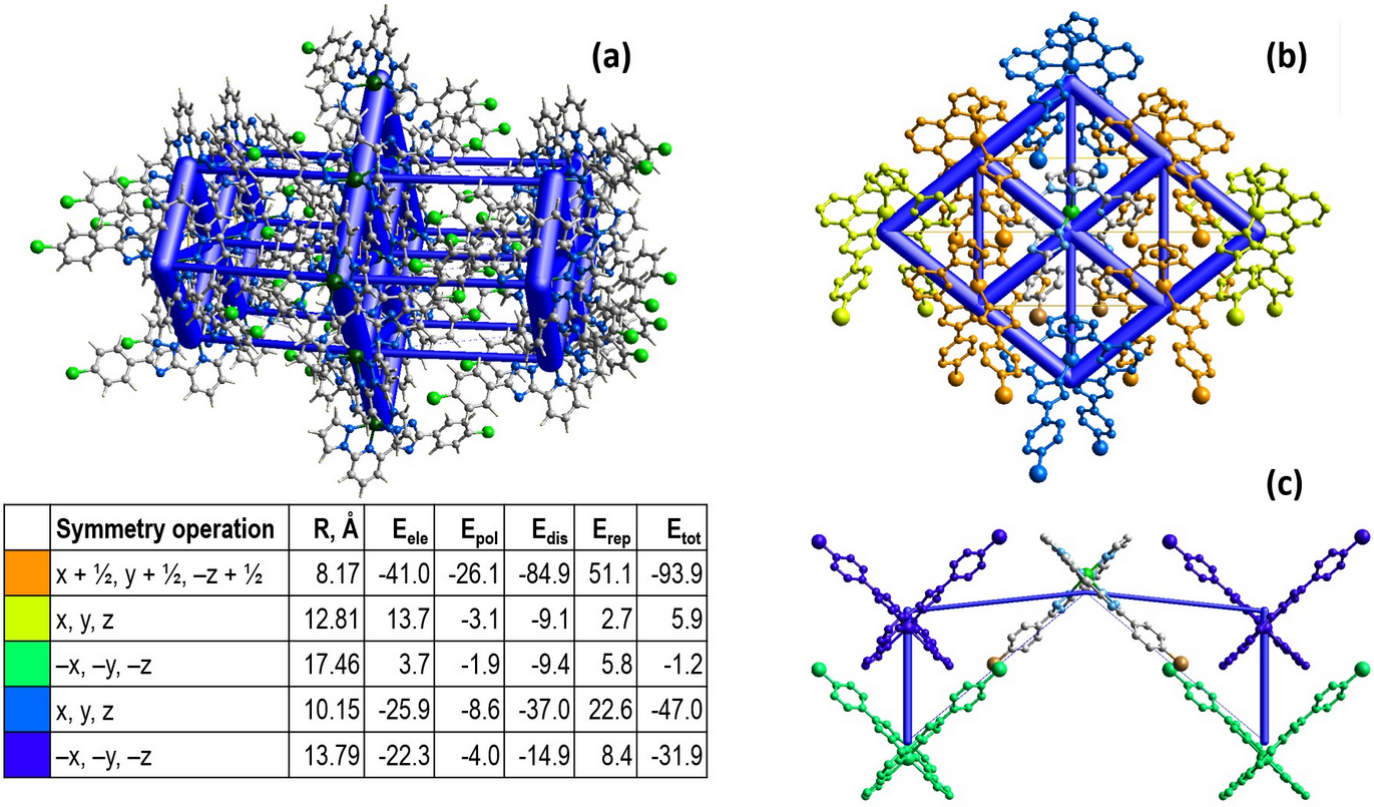

	Symmetry operation	R, Å	E_{ele}	E_{pol}	E_{dis}	E_{rep}	E_{tot}
	x + ½, y + ½, –z + ½	8.17	-41.0	-26.1	-84.9	51.1	-93.9
	x, y, z	12.81	13.7	-3.1	-9.1	2.7	5.9
	–x, –y, –z	17.46	3.7	-1.9	-9.4	5.8	-1.2
	x, y, z	10.15	-25.9	-8.6	-37.0	22.6	-47.0
	–x, –y, –z	13.79	-22.3	-4.0	-14.9	8.4	-31.9

Figure 5
(*a*) The calculated energy frameworks, showing the total energy diagrams (E_{tot}), (*b*) decomposition of the energy framework into the part corresponding to the interactions within a supramolecular layer and (*c*) interlayer interactions. In the table the corresponding colour-coded energy values E_{tot} are provided, including their E_{ele}, E_{pol}, E_{dis}, and E_{rep} components. Tube size is set at 100 scale, the blue colour corresponds to the attractive interaction, yellow to the repulsive interactions.

SOM; single-crystal measurements, SS; writing (original draft), MS; writing (review and editing of the manuscript), NK, MS; visualization and calculations, KZ, IOF; funding acquisition, IOF, NK, MS.

Funding information

Funding for this research was provided by: grants from the Ministry of Education and Science of Ukraine (grant Nos. 22BF037-03, 22BF037-04, 24BF037-03) and EURIZON project funded by the European Union (grant No. 871072).

References

Bonhommeau, S., Lacroix, P. G., Talaga, D., Bousseksou, A., Seredyuk, M., Fritsky, I. O. & Rodriguez, V. (2012). *J. Phys. Chem. C*, **116**, 11251–11255.

Chang, H. R., McCusker, J. K., Toftlund, H., Wilson, S. R., Trautwein, A. X., Winkler, H. & Hendrickson, D. N. (1990). *J. Am. Chem. Soc.* **112**, 6814–6827.

Dolomanov, O. V., Bourhis, L. J., Gildea, R. J., Howard, J. A. K. & Puschmann, H. (2009). *J. Appl. Cryst.* **42**, 339–341.

Drew, M. G. B., Harding, C. J., McKee, V., Morgan, G. G. & Nelson, J. (1995). *J. Chem. Soc. Chem. Commun.* pp. 1035–1038.

Groom, C. R., Bruno, I. J., Lightfoot, M. P. & Ward, S. C. (2016). *Acta Cryst.* B**72**, 171–179.

Grunwald, J., Torres, J., Buchholz, A., Näther, C., Kämmerer, L., Gruber, M., Rohlf, S., Thakur, S., Wende, H., Plass, W., Kuch, W. & Tuczek, F. (2023). *Chem. Sci.* **14**, 7361–7380.

Halcrow, M. A., Capel Berdiell, I., Pask, C. M. & Kulmaczewski, R. (2019). *Inorg. Chem.* **58**, 9811–9821.

Kershaw Cook, L. J., Mohammed, R., Sherborne, G., Roberts, T. D., Alvarez, S. & Halcrow, M. A. (2015). *Coord. Chem. Rev.* **289–290**, 2–12.

Piñeiro-López, L., Valverde-Muñoz, F. J., Seredyuk, M., Bartual-Murgui, C., Muñoz, M. C. & Real, J. A. (2018). *Eur. J. Inorg. Chem.* pp. 289–296.

Rigaku OD (2024). *CrysAlis PRO*. Rigaku Oxford Diffraction, Yarnton, England.

Senthil Kumar, K., Šalitroš, I., Heinrich, B., Fuhr, O. & Ruben, M. (2015). *J. Mater. Chem. C.* **3**, 11635–11644.

Seredyuk, M., Gaspar, A. B., Ksenofontov, V., Reiman, S., Galyametdinov, Y., Haase, W., Rentschler, E. & Gütlich, P. (2006). *Hyperfine Interact.* **166**, 385–390.

Seredyuk, M., Gaspar, A. B., Kusz, J., Bednarek, G. & Gütlich, P. (2007). *J. Appl. Cryst.* **40**, 1135–1145.

Seredyuk, M., Znovjyak, K., Valverde-Muñoz, F. J., da Silva, I., Muñoz, M. C., Moroz, Y. S. & Real, J. A. (2022). *J. Am. Chem. Soc.* **144**, 14297–14309.

Seredyuk, M., Znovjyak, K., Valverde-Muñoz, F. J., Muñoz, M. C., Fritsky, I. O. & Real, J. A. (2024). *Dalton Trans.* **53**, 8041–8049.

Table 3
Experimental details.

Crystal data	
Chemical formula	$[Ni(C_{16}H_{10}ClN_6)_2]\cdot 2CH_4O$
M_r	766.29
Crystal system, space group	Orthorhombic, *Pbcn*
Temperature (K)	200
a, *b*, *c* (Å)	12.8146 (4), 10.1523 (4), 27.5618 (10)
V (Å^3)	3585.7 (2)
Z	4
Radiation type	Mo *Kα*
μ (mm^{-1})	0.74
Crystal size (mm)	0.3 × 0.2 × 0.03
Data collection	
Diffractometer	Xcalibur, Eos
Absorption correction	Multi-scan (*CrysAlis PRO*; Rigaku OD, 2024)
T_{min}, T_{max}	0.982, 1.000
No. of measured, independent and observed [$I > 2\sigma(I)$] reflections	11432, 3169, 2460
R_{int}	0.040
(sin $\theta/\lambda)_{max}$ (Å^{-1})	0.595
Refinement	
$R[F^2 > 2\sigma(F^2)]$, $wR(F^2)$, *S*	0.042, 0.087, 1.05
No. of reflections	3169
No. of parameters	236
H-atom treatment	H atoms treated by a mixture of independent and constrained refinement
$\Delta\rho_{max}$, $\Delta\rho_{min}$ (e Å^{-3})	0.38, −0.43

Computer programs: *CrysAlis PRO* (Rigaku OD, 2024), *SHELXL2018/3* (Sheldrick, 2015) and *OLEX2* (Dolomanov *et al.*, 2009).

Seredyuk, M., Znovjyak, K. O., Kusz, J., Nowak, M., Muñoz, M. C. & Real, J. A. (2014). *Dalton Trans.* **43**, 16387–16394.

Sheldrick, G. M. (2015). *Acta Cryst.* C**71**, 3–8.

Shiga, T., Saiki, R., Akiyama, L., Kumai, R., Natke, D., Renz, F., Cameron, J. M., Newton, G. N. & Oshio, H. (2019). *Angew. Chem. Int. Ed.* **58**, 5658–5662.

Spackman, P. R., Turner, M. J., McKinnon, J. J., Wolff, S. K., Grimwood, D. J., Jayatilaka, D. & Spackman, M. A. (2021). *J. Appl. Cryst.* **54**, 1006–1011.

Suryadevara, N., Mizuno, A., Spieker, L., Salamon, S., Sleziona, S., Maas, A., Pollmann, E., Heinrich, B., Schleberger, M., Wende, H., Kuppusamy, S. K. & Ruben, M. (2022). *Chem. A Eur. J.* **28**, e202103853.

Wei, S. Y., Wang, J. L., Zhang, C. S., Xu, X.-T., Zhang, X. X., Wang, J. X. & Xing, Y.-H. (2015). *ChemPlusChem* **80**, 549-558.

Xing, N., Xu, L. T., Liu, X., Wu, Q., Ma, X. T. & Xing, Y. H. (2014). *ChemPlusChem* **79**, 1198-1207.

Yuan, L.-Z., Ge, Q., Zhao, X.-F., Ouyang, Y., Li, S.-H., Xie, C.-Z. & Xu, J.-Y. (2014). *Synth. React. Inorg. Met.-Org. Nano-Met. Chem.* **44**, 1175–1182.

supporting information

Acta Cryst. (2024). E**80**, 1235-1239 [https://doi.org/10.1107/S2056989024010338]

Crystal structure of bis{5-(4-chlorophenyl)-3-[6-(1*H*-pyrazol-1-yl)pyridin-2-yl]-1*H*-1,2,4-triazol-1-ido}nickel(II) methanol disolvate

Kateryna Znovjyak, Sergiu Shova, Dmitriy M. Panov, Nataliia S. Kariaka, Igor O. Fritsky, Sergey O. Malinkin and Maksym Seredyuk

Computing details

Bis{5-(4-chlorophenyl)-3-[6-(1*H*-pyrazol-1-yl)pyridin-2-yl]-1*H*-1,2,4-triazol-1-ido}nickel(II) methanol disolvate

Crystal data

$[Ni(C_{16}H_{10}ClN_6)_2]\cdot 2CH_4O$
$M_r = 766.29$
Orthorhombic, *Pbcn*
$a = 12.8146$ (4) Å
$b = 10.1523$ (4) Å
$c = 27.5618$ (10) Å
$V = 3585.7$ (2) Å^3
$Z = 4$
$F(000) = 1576$
$D_x = 1.419$ Mg m^{-3}
Mo $K\alpha$ radiation, $\lambda = 0.71073$ Å
Cell parameters from 3630 reflections
$\theta = 2.2$–$26.9°$
$\mu = 0.74$ mm^{-1}
$T = 200$ K
Plate, clear light colourless
0.3 × 0.2 × 0.03 mm

Data collection

Xcalibur, Eos diffractometer
Radiation source: fine-focus sealed X-ray tube, Enhance (Mo) X-ray Source
Graphite monochromator
Detector resolution: 16.1593 pixels mm^{-1}
ω scans
Absorption correction: multi-scan (CrysAlisPro; Rigaku OD, 2024)
$T_{min} = 0.982$, $T_{max} = 1.000$
11432 measured reflections
3169 independent reflections
2460 reflections with $I > 2\sigma(I)$
$R_{int} = 0.040$
$\theta_{max} = 25.0°$, $\theta_{min} = 2.2°$
$h = -15\rightarrow12$
$k = -8\rightarrow12$
$l = -28\rightarrow32$

Refinement

Refinement on F^2
Least-squares matrix: full
$R[F^2 > 2\sigma(F^2)] = 0.042$
$wR(F^2) = 0.087$
$S = 1.05$
3169 reflections
236 parameters
0 restraints
Hydrogen site location: mixed
H atoms treated by a mixture of independent and constrained refinement
$w = 1/[\sigma^2(F_o^2) + (0.0279P)^2 + 2.4046P]$ where $P = (F_o^2 + 2F_c^2)/3$
$(\Delta/\sigma)_{max} < 0.001$
$\Delta\rho_{max} = 0.38$ e Å^{-3}
$\Delta\rho_{min} = -0.43$ e Å^{-3}

Special details

Geometry. All esds (except the esd in the dihedral angle between two l.s. planes) are estimated using the full covariance matrix. The cell esds are taken into account individually in the estimation of esds in distances, angles and torsion angles; correlations between esds in cell parameters are only used when they are defined by crystal symmetry. An approximate (isotropic) treatment of cell esds is used for estimating esds involving l.s. planes.

Fractional atomic coordinates and isotropic or equivalent isotropic displacement parameters (Å²)

	x	*y*	*z*	U_{iso}*/U_{eq}
Ni1	0.500000	0.69121 (4)	0.750000	0.02084 (14)
Cl1	0.65525 (9)	0.02490 (10)	0.48765 (3)	0.0732 (3)
N4	0.56268 (15)	0.5528 (2)	0.70190 (7)	0.0232 (5)
N3	0.65534 (14)	0.6994 (2)	0.76563 (7)	0.0213 (5)
N6	0.70584 (15)	0.4439 (2)	0.67758 (7)	0.0260 (5)
O1	0.35256 (17)	0.5580 (2)	0.61839 (9)	0.0536 (7)
N1	0.51184 (15)	0.8366 (2)	0.80671 (8)	0.0254 (5)
N2	0.61374 (15)	0.8598 (2)	0.82014 (8)	0.0248 (5)
N5	0.53272 (16)	0.4702 (2)	0.66553 (8)	0.0261 (5)
C9	0.66590 (18)	0.5348 (2)	0.70733 (9)	0.0225 (6)
C11	0.6257 (2)	0.3115 (3)	0.61194 (9)	0.0286 (6)
C10	0.62050 (19)	0.4072 (2)	0.65185 (9)	0.0240 (6)
C4	0.69229 (18)	0.7853 (2)	0.79721 (9)	0.0226 (6)
C8	0.72106 (18)	0.6191 (2)	0.74160 (9)	0.0232 (6)
C1	0.4560 (2)	0.9114 (3)	0.83634 (9)	0.0278 (6)
H1	0.381914	0.915928	0.836126	0.033*
C5	0.79770 (19)	0.8008 (3)	0.80689 (10)	0.0308 (7)
H5	0.822378	0.864474	0.829382	0.037*
C12	0.7100 (2)	0.2265 (3)	0.60884 (10)	0.0387 (7)
H12	0.762240	0.228747	0.633302	0.046*
C15	0.5598 (3)	0.2190 (3)	0.53748 (10)	0.0409 (8)
H15	0.508238	0.216511	0.512739	0.049*
C16	0.5500 (2)	0.3065 (3)	0.57582 (10)	0.0346 (7)
H16	0.491181	0.363367	0.577433	0.041*
C14	0.6440 (3)	0.1360 (3)	0.53531 (10)	0.0410 (8)
C3	0.6197 (2)	0.9480 (3)	0.85679 (10)	0.0341 (7)
H3	0.681449	0.979665	0.871858	0.041*
C7	0.82769 (19)	0.6262 (3)	0.74938 (10)	0.0316 (7)
H7	0.874286	0.569090	0.732760	0.038*
C2	0.5197 (2)	0.9827 (3)	0.86793 (11)	0.0373 (7)
H2	0.497898	1.043138	0.892220	0.045*
C13	0.7197 (3)	0.1382 (3)	0.57077 (11)	0.0464 (8)
H13	0.777684	0.080013	0.569161	0.056*
C6	0.8646 (2)	0.7190 (3)	0.78215 (10)	0.0352 (7)
H6	0.937557	0.726096	0.787585	0.042*
C17	0.3810 (3)	0.6355 (4)	0.57866 (13)	0.0666 (11)
H17A	0.401889	0.578408	0.551683	0.100*
H17B	0.439474	0.692602	0.587693	0.100*
H17C	0.321473	0.689799	0.568711	0.100*

H1A	0.407 (3)	0.529 (3)	0.6315 (12)	0.062 (11)*

Atomic displacement parameters (Å²)

	U^{11}	U^{22}	U^{33}	U^{12}	U^{13}	U^{23}
Ni1	0.0141 (2)	0.0264 (3)	0.0220 (3)	0.000	−0.00045 (19)	0.000
Cl1	0.1083 (8)	0.0673 (7)	0.0441 (6)	0.0039 (6)	0.0019 (5)	−0.0299 (5)
N4	0.0192 (11)	0.0277 (12)	0.0226 (12)	−0.0017 (9)	−0.0003 (9)	−0.0023 (10)
N3	0.0172 (10)	0.0247 (12)	0.0219 (12)	−0.0013 (9)	−0.0013 (8)	0.0004 (10)
N6	0.0214 (11)	0.0309 (13)	0.0257 (12)	0.0007 (9)	−0.0002 (9)	−0.0073 (10)
O1	0.0324 (13)	0.0715 (17)	0.0569 (16)	−0.0044 (12)	−0.0083 (11)	0.0242 (13)
N1	0.0172 (11)	0.0318 (13)	0.0273 (12)	0.0025 (9)	−0.0012 (9)	0.0001 (10)
N2	0.0190 (11)	0.0281 (12)	0.0273 (12)	0.0009 (9)	−0.0016 (9)	−0.0066 (11)
N5	0.0234 (12)	0.0288 (13)	0.0261 (13)	−0.0031 (9)	−0.0016 (9)	−0.0038 (11)
C9	0.0182 (13)	0.0261 (15)	0.0231 (14)	−0.0005 (10)	0.0000 (11)	−0.0007 (12)
C11	0.0332 (15)	0.0261 (15)	0.0264 (15)	−0.0059 (12)	0.0032 (12)	−0.0007 (13)
C10	0.0248 (14)	0.0249 (14)	0.0223 (14)	−0.0023 (11)	0.0000 (11)	−0.0011 (12)
C4	0.0211 (13)	0.0236 (14)	0.0230 (14)	−0.0006 (11)	−0.0002 (11)	−0.0034 (12)
C8	0.0204 (13)	0.0252 (14)	0.0239 (14)	0.0014 (11)	0.0032 (11)	−0.0013 (12)
C1	0.0218 (13)	0.0344 (16)	0.0271 (16)	0.0081 (12)	0.0020 (12)	0.0005 (13)
C5	0.0222 (14)	0.0355 (16)	0.0347 (16)	−0.0032 (12)	−0.0032 (12)	−0.0118 (14)
C12	0.0413 (18)	0.0392 (18)	0.0357 (17)	0.0035 (14)	−0.0053 (14)	−0.0104 (15)
C15	0.058 (2)	0.0399 (19)	0.0250 (16)	−0.0099 (16)	−0.0079 (14)	0.0027 (15)
C16	0.0413 (17)	0.0325 (17)	0.0299 (16)	−0.0039 (14)	−0.0024 (13)	−0.0007 (14)
C14	0.064 (2)	0.0343 (18)	0.0248 (16)	−0.0042 (16)	0.0065 (15)	−0.0068 (14)
C3	0.0307 (15)	0.0366 (17)	0.0351 (17)	−0.0001 (13)	−0.0034 (13)	−0.0123 (15)
C7	0.0181 (13)	0.0383 (16)	0.0385 (17)	0.0034 (11)	−0.0015 (12)	−0.0111 (15)
C2	0.0333 (17)	0.0425 (18)	0.0360 (17)	0.0097 (13)	0.0023 (13)	−0.0128 (15)
C13	0.052 (2)	0.0437 (19)	0.0432 (19)	0.0106 (16)	0.0036 (16)	−0.0111 (16)
C6	0.0138 (13)	0.0484 (19)	0.0434 (18)	−0.0013 (12)	−0.0026 (12)	−0.0089 (16)
C17	0.082 (3)	0.057 (2)	0.061 (3)	−0.014 (2)	−0.015 (2)	0.017 (2)

Geometric parameters (Å, º)

Ni1—N4^{i}	2.092 (2)	C4—C5	1.386 (3)
Ni1—N4	2.092 (2)	C8—C7	1.385 (3)
Ni1—N3	2.0383 (19)	C1—H1	0.9500
Ni1—N3^{i}	2.0384 (19)	C1—C2	1.396 (4)
Ni1—N1	2.155 (2)	C5—H5	0.9500
Ni1—N1^{i}	2.155 (2)	C5—C6	1.374 (4)
Cl1—C14	1.737 (3)	C12—H12	0.9500
N4—N5	1.363 (3)	C12—C13	1.386 (4)
N4—C9	1.344 (3)	C15—H15	0.9500
N3—C4	1.320 (3)	C15—C16	1.386 (4)
N3—C8	1.346 (3)	C15—C14	1.371 (4)
N6—C9	1.337 (3)	C16—H16	0.9500
N6—C10	1.355 (3)	C14—C13	1.377 (4)
O1—C17	1.396 (4)	C3—H3	0.9500

O1—H1A	0.84 (3)	C3—C2	1.363 (4)
N1—N2	1.378 (3)	C7—H7	0.9500
N1—C1	1.325 (3)	C7—C6	1.388 (4)
N2—C4	1.409 (3)	C2—H2	0.9500
N2—C3	1.352 (3)	C13—H13	0.9500
N5—C10	1.347 (3)	C6—H6	0.9500
C9—C8	1.458 (3)	C17—H17A	0.9800
C11—C10	1.470 (4)	C17—H17B	0.9800
C11—C12	1.386 (4)	C17—H17C	0.9800
C11—C16	1.392 (4)		

N4—Ni1—N4^{i}	95.63 (11)	N3—C8—C9	111.8 (2)
N4^{i}—Ni1—N1	91.57 (8)	N3—C8—C7	120.6 (2)
N4—Ni1—N1^{i}	91.58 (8)	C7—C8—C9	127.5 (2)
N4—Ni1—N1	153.19 (7)	N1—C1—H1	124.3
N4^{i}—Ni1—N1^{i}	153.19 (7)	N1—C1—C2	111.4 (2)
N3—Ni1—N4	77.66 (8)	C2—C1—H1	124.3
N3^{i}—Ni1—N4^{i}	77.66 (8)	C4—C5—H5	121.8
N3^{i}—Ni1—N4	105.57 (8)	C6—C5—C4	116.3 (2)
N3—Ni1—N4^{i}	105.58 (8)	C6—C5—H5	121.8
N3—Ni1—N3^{i}	175.32 (12)	C11—C12—H12	119.4
N3—Ni1—N1	75.52 (8)	C11—C12—C13	121.3 (3)
N3^{i}—Ni1—N1	101.19 (8)	C13—C12—H12	119.4
N3—Ni1—N1^{i}	101.19 (8)	C16—C15—H15	120.0
N3^{i}—Ni1—N1^{i}	75.52 (8)	C14—C15—H15	120.0
N1^{i}—Ni1—N1	93.53 (11)	C14—C15—C16	119.9 (3)
N5—N4—Ni1	140.50 (15)	C11—C16—H16	119.8
C9—N4—Ni1	113.52 (16)	C15—C16—C11	120.3 (3)
C9—N4—N5	105.97 (19)	C15—C16—H16	119.8
C4—N3—Ni1	121.12 (16)	C15—C14—Cl1	119.8 (2)
C4—N3—C8	120.0 (2)	C15—C14—C13	120.9 (3)
C8—N3—Ni1	118.84 (16)	C13—C14—Cl1	119.3 (3)
C9—N6—C10	101.6 (2)	N2—C3—H3	126.7
C17—O1—H1A	108 (2)	N2—C3—C2	106.7 (2)
N2—N1—Ni1	112.27 (14)	C2—C3—H3	126.7
C1—N1—Ni1	143.26 (18)	C8—C7—H7	120.9
C1—N1—N2	104.4 (2)	C8—C7—C6	118.2 (2)
N1—N2—C4	117.7 (2)	C6—C7—H7	120.9
C3—N2—N1	111.6 (2)	C1—C2—H2	127.0
C3—N2—C4	130.6 (2)	C3—C2—C1	106.0 (2)
C10—N5—N4	105.23 (19)	C3—C2—H2	127.0
N4—C9—C8	118.0 (2)	C12—C13—H13	120.5
N6—C9—N4	113.8 (2)	C14—C13—C12	119.0 (3)
N6—C9—C8	128.1 (2)	C14—C13—H13	120.5
C12—C11—C10	119.6 (2)	C5—C6—C7	121.4 (2)
C12—C11—C16	118.5 (3)	C5—C6—H6	119.3
C16—C11—C10	121.9 (2)	C7—C6—H6	119.3
N6—C10—C11	122.4 (2)	O1—C17—H17A	109.5

N5—C10—N6	113.4 (2)	O1—C17—H17B	109.5
N5—C10—C11	124.1 (2)	O1—C17—H17C	109.5
N3—C4—N2	113.2 (2)	H17A—C17—H17B	109.5
N3—C4—C5	123.5 (2)	H17A—C17—H17C	109.5
C5—C4—N2	123.3 (2)	H17B—C17—H17C	109.5
Ni1—N4—N5—C10	−178.80 (19)	C9—N6—C10—N5	−1.1 (3)
Ni1—N4—C9—N6	178.29 (16)	C9—N6—C10—C11	176.9 (2)
Ni1—N4—C9—C8	−5.4 (3)	C9—C8—C7—C6	176.6 (3)
Ni1—N3—C4—N2	4.2 (3)	C11—C12—C13—C14	0.4 (5)
Ni1—N3—C4—C5	−175.7 (2)	C10—N6—C9—N4	1.4 (3)
Ni1—N3—C8—C9	−0.9 (3)	C10—N6—C9—C8	−174.6 (3)
Ni1—N3—C8—C7	176.8 (2)	C10—C11—C12—C13	−177.6 (3)
Ni1—N1—N2—C4	−2.1 (3)	C10—C11—C16—C15	177.0 (2)
Ni1—N1—N2—C3	−178.00 (17)	C4—N3—C8—C9	−178.1 (2)
Ni1—N1—C1—C2	176.5 (2)	C4—N3—C8—C7	−0.5 (4)
Cl1—C14—C13—C12	−179.6 (2)	C4—N2—C3—C2	−174.7 (3)
N4—N5—C10—N6	0.4 (3)	C4—C5—C6—C7	0.0 (4)
N4—N5—C10—C11	−177.5 (2)	C8—N3—C4—N2	−178.6 (2)
N4—C9—C8—N3	4.2 (3)	C8—N3—C4—C5	1.5 (4)
N4—C9—C8—C7	−173.3 (3)	C8—C7—C6—C5	0.9 (4)
N3—C4—C5—C6	−1.2 (4)	C1—N1—N2—C4	175.2 (2)
N3—C8—C7—C6	−0.7 (4)	C1—N1—N2—C3	−0.7 (3)
N6—C9—C8—N3	180.0 (2)	C12—C11—C10—N6	19.7 (4)
N6—C9—C8—C7	2.5 (4)	C12—C11—C10—N5	−162.5 (3)
N1—N2—C4—N3	−1.1 (3)	C12—C11—C16—C15	−0.6 (4)
N1—N2—C4—C5	178.9 (2)	C15—C14—C13—C12	−0.4 (5)
N1—N2—C3—C2	0.5 (3)	C16—C11—C10—N6	−157.9 (3)
N1—C1—C2—C3	−0.4 (3)	C16—C11—C10—N5	19.9 (4)
N2—N1—C1—C2	0.7 (3)	C16—C11—C12—C13	0.1 (4)
N2—C4—C5—C6	178.9 (2)	C16—C15—C14—Cl1	179.1 (2)
N2—C3—C2—C1	0.0 (3)	C16—C15—C14—C13	−0.1 (5)
N5—N4—C9—N6	−1.2 (3)	C14—C15—C16—C11	0.6 (4)
N5—N4—C9—C8	175.2 (2)	C3—N2—C4—N3	173.9 (2)
C9—N4—N5—C10	0.4 (3)	C3—N2—C4—C5	−6.2 (4)

Symmetry code: (i) −*x*+1, *y*, −*z*+3/2.

Hydrogen-bond geometry (Å, º)

D—H···*A*	*D*—H	H···*A*	*D*···*A*	*D*—H···*A*
C2—H2···C14^{ii}	0.95	2.86	3.73 (4)	153
C2—H2···C15^{ii}	0.95	2.74	3.686 (4)	178
C2—H2···C16^{ii}	0.95	2.88	3.743 (4)	151
C3—H3···O1^{iii}	0.95	2.35	3.259 (4)	160
C5—H5···O1^{iii}	0.95	2.47	3.399 (4)	167
C1—H1···N6^{iv}	0.95	2.31	3.245 (6)	170

C7—H7···C1^{iv}	0.95	2.70	3.611 (4)	161
O1—H1*A*···N5	0.84	1.96	2.795 (6)	176

Symmetry codes: (ii) −*x*+1, *y*+1, −*z*+3/2; (iii) *x*+1/2, *y*+1/2, −*z*+3/2; (iv) *x*−1/2, *y*+1/2, −*z*+3/2.